Journal of Solid State Chemistry 184 (2011) 2220–2230

Contents lists available at ScienceDirect

Journal of Solid State Chemistry

journal homepage: www.elsevier.com/locate/jssc

The binary tin-rich lanthanum stannides La_2Sn_5 and La_3Sn_7—A structural and bond theoretical study

Ines Dürr, Michael Schwarz, Caroline Röhr *

Institut für Anorganische und Analytische Chemie, University of Freiburg, Albertstr. 21, D-79104 Freiburg, Germany

ARTICLE INFO

Article history:
Received 8 March 2011
Received in revised form
20 June 2011
Accepted 26 June 2011
Available online 1 July 2011

Keywords:
Stannides
Lanthanum
Crystal structure
Band structure calculation

ABSTRACT

The three tin-rich lanthanum stannides $LaSn_3$, La_2Sn_5 and La_3Sn_7, which were known only from indexed powder diagrams, have been synthesized from melts of the elements by slow cooling of sealed sample tubes or arc melting and quenching. Their crystal structures were refined from X-ray powder diffractometer data using the Rietveld method. $LaSn_3$ (cubic, space group $Pm\bar{3}m$, $a=477.77(1)$ pm, $Z=1$, $R_{F^2}=0.044$) crystallizes with the common Cu_3Au structure type, which can be described either as an ordered close packing or as a network of $[Sn_6]$ octahedra (*closo* clusters) connected via common vertices. The structures of La_2Sn_5 (Ce_2Sn_5 structure type, orthorhombic, space group *Cmmm*, $a=463.85(3)$, $b=3581.3(3)$, $c=469.83(4)$ pm, $Z=4$, $R_{F^2}=0.075$) and La_3Sn_7 (Gd_3Sn_7 structure type, orthorhombic, space group *Cmmm*, $a=457.83(4)$, $b=2628.40(2)$, $c=467.99(4)$ pm, $Z=2$, $R_{F^2}=0.068$), which retain some similarities to ordered close packings as well, show 2D blocks of corner-sharing $[Sn_6]$ octahedra terminated by $[Sn_5]$ square pyramids (*nido* clusters). In between these layers, isolated Sn zigzag chains similar to those observed in LaSn (CrB structure type) are interspersed. A simple v.e. count after Zintl and Wade/Jemmis for the polyanionic Sn building blocks resulting from these structure descriptions fits the observed v.e. numbers of the three compounds almost exactly. It is also possible to explain the minima of the tDOS close to E_F, which have been calculated within the framework of the FP-LAPW DFT approach. However, the simple assumption of an exclusively Sn-*p* bonded polyanion would neglect the large Sn–La bonding contributions and the reduced amount of electron transfer from La to Sn when compared to related alkaline earth stannides.

1. Introduction

Tin-rich alkaline earth stannides are interesting intermetallics to investigate not only the validity of simple electron counting rules like the Zintl concept [1–3] and Wade's rules [4,5], but also the structural and electronic transition to genuine alloys [6,7]. This can be seen from the fact that their structures, *e.g.* $CaSn_3$ (Cu_3Au structure type), can be alternatively interpreted in terms of superstructures of the cubic close packing or as condensed octahedral clusters. In accordance with the latter, the electronic structures show *pseudo* bandgaps at or near the fermi level and the valence electron numbers can be explained using the Wade/Jemmis electron counting rules for condensed clusters.

The exchange of the alkaline earth metal calcium against the more electron rich rare earth element lanthanum allows the variation of the valence electron (v.e.) numbers without a significant change in the radius ratios (ionic radii: $r\,(La^{3+})=136$ pm; $r\,(Ca^{2+})=134$ pm, CN=12, after Shannon, [8]). In addition, the trielides and tetrelides of lanthanum and the alkaline earths calcium and strontium show some similarities in their crystal chemistry. In contrast to the extensively studied compounds of the later *f* elements, lanthanum in its positive oxidation state offers the additional advantage that its *f* states, which are otherwise difficult to correctly treat in band structure calculations, are unoccupied.

2. Literature data on La–Sn phases

Thermoanalytic studies of the binary system La–Sn dating from 1988, 1992 and 2000 [9–11] report no less than seven intermetallic phases (in bracket: Sn:La ratio and melting behavior: c/p=congruent/peritectic melting)): La_5Sn_3 (0.60, p), La_5Sn_4 (0.80, c), $La_{11}Sn_{10}$ (0.91, p), LaSn (1.0, p), La_2Sn_3 (1.5, p), La_3Sn_5 (1.67, c) and $LaSn_3$ (3.0, c). Further compounds mentioned in other works [12–14] are $LaSn_2$ (2.0), La_3Sn_7 (2.33) and La_2Sn_5 (2.5), which are probably peritectic melting phases in between the two congruently melting stannides La_3Sn_5 (1.67) and $LaSn_3$ (3.0).

* Corresponding author.
E-mail address: caroline@ruby.chemie.uni-freiburg.de (C. Röhr).

0022-4596/$ - see front matter © 2011 Elsevier Inc. All rights reserved.
doi:10.1016/j.jssc.2011.06.035

Up to now only two of the binary La–Sn compounds reported in the literature have been structurally characterized by means of single crystal data. These two phases, the congruently melting stannide La_3Sn_5 crystallizing with the Pu_3Pd_5 structure type [15] and the singular phase La_2Sn_3 (triclinic, own structure type [16]) are so similar in stoichiometry (Sn:La ratio 1.67 and 1.5), that they represent only a small part of the phase diagram. Lanthanum stannides richer in La are either known or assumed not to be pure binary phases, instead containing additional interstitial atoms like oxygen, nitrogen or hydrogen, and forming structure types like Mn_5Si_3 and W_5Si_3, that provide suitable voids for the incorporation of anions of these light atoms [17,18]. The structures of the compounds at an approximately 1:1 composition like $La_{11}Sn_{10}$ ($Ho_{11}Ge_{10}$ structure type), La_5Sn_4 (Sm_5Ge_4 type) and LaSn (CrB type) were only assigned their structure types using powder data [9]. Single crystal structure determinations and calculations of the electronic structures are currently in progress [19]. The Sn-richest stannide $LaSn_3$ crystallizes with the simple cubic Cu_3Au structure type. Due to its superconducting properties this compound has been the topic of a large number of experimental and theoretical studies in the seventies and early eighties ([20–24] and references therein).

In contrast, our knowledge concerning the structure of La_3Sn_7, La_2Sn_5 and $LaSn_2$ is very limited: Apart from a short reference on La_2Sn_5 in [13] (1983) and a recent confirmation of the existence of this compound [25] structural information on the three stannides are collected in a paper by Weitzer, Hiebl and Rogl in 1992 [12] exclusively. In that work, which mainly deals with the magnetic properties of the respective Pr and Nd compounds, the isotypism of La_3Sn_7 and La_2Sn_5 with the cerium stannides [26] is realized from their powder patterns and the compounds are thus assigned to the structure types Ce_2Sn_5 (*oS*28) and Ce_3Sn_7/Gd_3Sn_7 (*oS*28), all space group *Cmmm*. The authors inferred, that $LaSn_2$ does not form the $ZrSi_2$ structure type observed for the late rare earth elements, but should form the $ZrGa_2$ structure type (*oS*12, space group *Cmmm*) instead. The lattice constants of all three phases have been refined using powder data and the structures were described as superstructures of $LaSn_3$ according to Boucherle et al. [26], who solved the structures of the analogous Ce stannides by means of single crystal neutron data. In 1994, several physical properties (*e.g.* electrical resistivity) of La_3Sn_7 and La_2Sn_5 have been measured for comparison with the magnetic ordered cerium stannides [14].

3. Experimental section

3.1. Preparation

The synthesis of the La stannides was generally performed starting from the elements lanthanum and tin obtained from commercial sources and used without further purification (La: Aldrich, 99% and Sn: ABCR Karlsruhe, 99.9%). Due to the unknown melting behavior and the probability of peritectic decomposition slightly below 1115 °C inferred from the phase diagram, several samples have been prepared by slow cooling from maximum temperatures in the range 1000–1400 °C as well as by quenching after arc melting. For the furnace preparations, the educts (*approx.*1 g) were filled into tantalum crucibles under an argon atmosphere. The sealed containers were heated in corundum tubes under a static Ar atmosphere to maximum temperatures between 1000 and 1400 °C with constant heating/cooling rates given in Table 1 for all samples. For the arc-melted samples, a sample of about 100 mg of the two elements was weighed under argon, transferred to the water-cooled copper crucible plate of a vacuum arc melter, evacuated and arc-melted at low pressure helium atmosphere. After both preparations, representative parts of the reguli were ground in Ar atmosphere and sealed in capillaries with a diameter of 0.3 mm. X-ray powder diagrams were collected on a transmission powder diffractometer system (STADI P, linear PSD, Fa. Stoe & Cie, Darmstadt, Mo$K_{\alpha 1}$ radiation, germanium monochromator).

The congruently melting tristannide $LaSn_3$ can be synthesized from stoichiometric or tin-rich melts (Table 1, sample no. 1), in the latter case a small excess of metallic tin was detected in the powder patterns. To the La-rich side of $LaSn_3$ (no. 2: $LaSn_{2.7}$) both the stannides La_3Sn_7 and La_2Sn_5 have been first detected in the powder diagram of an arc-melted sample. As obvious from the Rietveld refinements in Fig. 1, the differentiation between these two structurally related compounds (and $LaSn_3$ as well) is possible only on the basis of the reflections (0,14,0) (La_2Sn_5) and (0,10,0)/(1,7,1) (La_3Sn_7). A pure sample of $LaSn_3$, the powder diagram of which was used for the Rietveld refinement (Chapter 3.2), was initially obtained from a somewhat La-richer sample (3a, Table 1) originally intended to synthesize La_2Sn_5. Due to the slow cooling rate of only 1 °C/h loss of small amounts of La by evaporation can be assumed. The same sample composition subjected to a maximum temperature of 1400 °C and a faster

Table 1
Details of the synthesis of the lanthanum stannides, together with the analysis of the phase composition from powder diffractometer data.

No.	Sample	Weighed sample				T program					Phase composition (powder data)			
	composition	La (mg)	(mmol)	Sn (mg)	(mmol)	$\dot{T}_{\uparrow}$ (°C/h)	T_{max} (°C)	$\dot{T}_{\downarrow}$ (°C/h)	T (°C)	$\dot{T}_{\downarrow}$ (°C/h)	La_3Sn_5 (Pu_3Pd_5)	La_3Sn_7 (Gd_3Sn_7)	La_2Sn_5 (Ce_2Sn_5)	$LaSn_3$ (Cu_3Au)
1	$LaSn_4$	226.3	1.629	773.7	6.518	200	1200	20	400	200				×
2	$LaSn_{2.7}$	30.2	0.217	69.6	0.585	arc melting						×	×	×
3*a*	$LaSn_{2.5}$	318.8	2.295	681.2	5.738	200	1000	1	800	200				×
3*b*	$LaSn_{2.5}$	318.8	2.295	681.3	5.739	200	1400	20	400	200			×	×
4*a*	$LaSn_{2.33}$	333.9	2.404	666.0	5.610	200	1400	20	400	200			×	
4*b*	$LaSn_{2.33}$	167.1	1.203	333.0	2.805	200	1200	20	400	200		×	×	
5	$LaSn_{2.2}$	34.7	0.250	65.4	0.551	arc melting						×		
6*a*	$LaSn_2$	369.2	2.659	630.9	5.315	200	1050	5	700	200			×	(×)
6*b*	$LaSn_2$	369.1	2.657	630.9	5.315	200	1200	20	400	200	×		×	
6*c*	$LaSn_2$	377.0	2.714	631.0	5.32?	200	1400	20	400	200	(×)	×		
6*d*	$LaSn_2$	37.0	0.266	63.1	0.532	arc melting					×	×		
7	$LaSn_{1.67}$	41.1	0.296	58.7	0.494	arc melting					×			
8*a*	$LaSn_{1.5}$	438.2	3.155	561.7	4.732	200	1200	20	400	200	×		(×)	
8*b*	$LaSn_{1.5}$	43.9	0.316	56.2	0.473	arc melting					×			

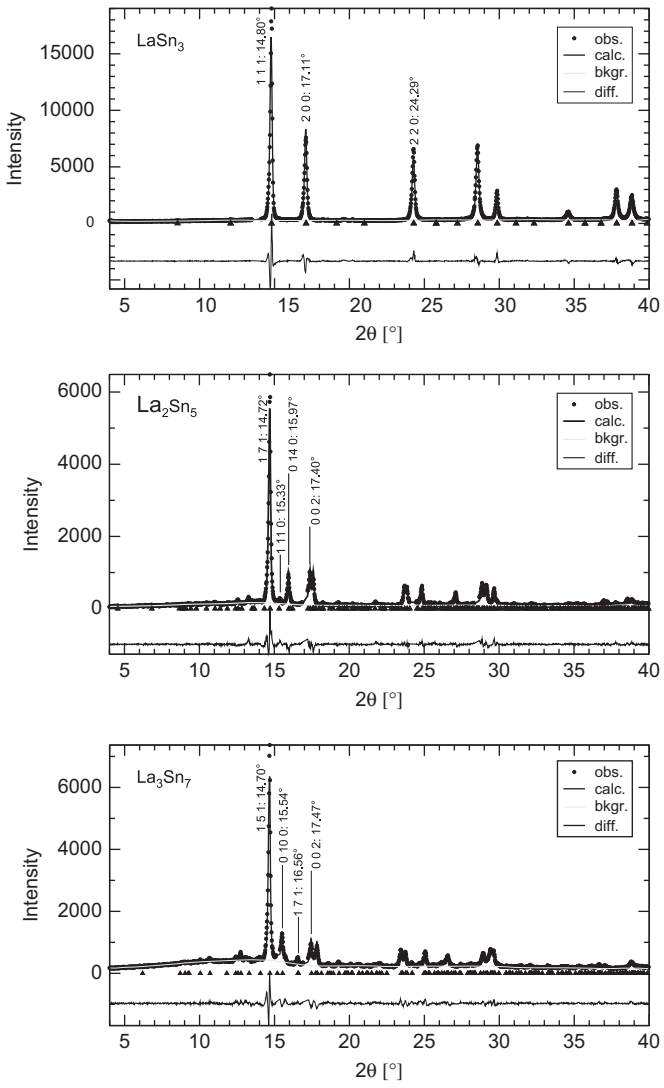

Fig. 1. Results of the Rietveld refinements of $LaSn_3$ (above), La_2Sn_5 (middle) and La_3Sn_7 (below) [27,28] (Characteristic reflections are indexed).

cooling rate succeeded in the expected parallel syntheses of $LaSn_3$ and La_2Sn_5 (sample 3b). From melts of overall composition La_3Sn_7 (70% Sn, no. 4a/b) both La_2Sn_5 and La_3Sn_7 are accessible. According to the phase diagram of the cerium analog, quenching of these samples (*cf.* no. 5) gives the 3:7 compound in pure phase, whereas slow cooling results in the formation of La_2Sn_5 only (4*a*) or of mixtures of the 2:5 and the 3:7 stannide (4*b*). From the latter sample, crystals of both compounds La_2Sn_5 and La_3Sn_7 suitable for a preliminary single crystal structure refinements could be recovered (Chapter 3.3). At a 1:2 composition (66.7% Sn), *i.e.* slightly to the left of the two title compounds in the phase diagram, the tin-rich stannide La_2Sn_5 is formed at 1050 °C (sample no. 6a), a clear indication that La_2Sn_5 exhibits the higher peritectic temperature compared to La_3Sn_7. The latter is only formed on quenching (sample no. 6d), as expected together with the Pu_3Pd_5-type phase La_3Sn_5 [15]. This very stable stannide is also formed in pure phase from all samples with Sn proportions in the range 62.5%–60%.

3.2. Rietveld powder refinement

The title compounds could not be obtained in the form of crystals of adequate size and quality for a satisfying single crystal structure analysis (Chapter 3.3). Therefore, X-ray powder diagrams with long exposure times were used to refine the structure parameters by the Rietveld method as implemented in the programs GSAS [27] and EXPGUI [28].

For the cubic phase $LaSn_3$, the powder diagram of the pure phase sample 3a was used to refine the lattice parameter and the thermal parameters of La and Sn. The full-pattern refinement converged at good profile and structure *R* factors of $R_p = 0.086$ and $R_{F^2} = 0.044$. The lattice parameter obtained ($a = 477.77(1)$ pm) is in good agreement with the value 476.9 pm reported in [29]. The results of the refinement are collected in Table 2 and Fig. 1.

The structure of La_2Sn_5 was refined using a powder pattern of sample 6a. Starting parameters used were those of Ce_2Sn_5 [26]. Due to minute contamination with $LaSn_3$ the introduction of three small 'excluded regions' (s. Table 2) was necessary. The refinement of nine structure and four profile parameters smoothly converged at $R_{F^2} = 0.075$. The refined lattice parameters (Table 3) are in accordance with those reported in the literature [12] ($a = 462.3$, $b = 3574.3(7)$ and $c = 468.18(8)$ pm) and with the single crystal values ($a = 462.1$, $b = 3579.5$ and $c = 468.8$ pm). This also holds for the atomic parameters when comparing the results of the Rietveld refinement, the single crystal structure analysis and the values of the isotypic neodymium stannide. The maximum parameter difference is in the third decimal place, corresponding to distance changes of no more than 1 pm (Result *cf.* Fig. 1 (center) and Table 3).

The powder pattern of La_3Sn_7 (Gd_3Sn_7 structure type [30]) obtained from the quenched sample 5 has been refined in a similar manner using the atom parameters of the gadolinium phase. The lattice parameters obtained ($a = 457.83(4)$, $b = 2628.40(2)$, $c = 467.99(4)$ pm) are in accordance with the literature values ($a = 456.4$, $b = 2615.6$, $c = 467.1(1)$ pm, [12]) and also fit those of the single crystal investigation ($a = 459.2$, $b = 2618.9$, $c = 468.13$ pm). The full-pattern refinement converged to a Bragg-*R* value of 0.068, details are collected in Table 3 and depicted in Fig. 1 (bottom).

3.3. Single crystal structure refinement

Complementary to the Rietveld refinements, the crystal structures of La_2Sn_5 and La_3Sn_7 have been also analyzed by means of single crystal data. For this task, platelets of silver metallic luster of both compounds were selected from the sample 4b (Table 1). They were mounted in glass capillaries (diameter 0.1 mm) under dried paraffine oil and centered on a diffractometer equipped with an image plate area detector. The diffraction data obtained showed the expected orthorhombic *C* centered lattice with lattice parameters consistent with those obtained from the powder refinements (Chapter 3.2). Starting from the structural model of the cerium compounds [26] (space group *Cmmm*) the least squares refinements (program SHELXL-97 [31,32]) converged to *R*1 values of about 20%. The poor crystal quality, also reportedly a problem in several related phases [26], is clearly responsible for these high *R* factors. The results of the single crystal structure analysis are nevertheless mentioned here (*cf.* also Supplemental Data) to support the correct indexing of the powder diagrams is view of the superstructure relation between $LaSn_3$ and La_2Sn_5/La_3Sn_7. Due to the poor single crystal structure refinements and the good quality of the Rietveld analyses the results of the powder data were used for all further discussions and also for the calculation of the band structures.

3.4. Band structure calculations

For the compounds $LaSn_3$ (and $CaSn_3$ in comparison [33,6]), La_2Sn_5 and La_3Sn_7, DFT calculations of the electronic band structures were performed using the FP-LAPW method (program

Table 2
Crystallographic data, details of the data collection and the Rietveld refinement for the stannides $LaSn_3$, La_2Sn_5 and La_3Sn_7.

Compound		$LaSn_3$	La_2Sn_5	La_3Sn_7
Structure type		Cu_3Au	Ce_2Sn_5	Gd_3Sn_7
Person code		*cP*4	*oS*28	*oS*20
Crystal system		cubic	orthorhombic	
Space group		*Pm* $\bar{3}$*m*, No. 221	*Cmmm*, No. 65	
Lattice constants (pm)	*a*	477.77(1)	463.85(3)	457.83(4)
	b	–	3581.3(3)	2628.40(2)
	c	–	469.83(4)	467.99(4)
Volume of the u.c. (10^6pm^3)		109.06(1)	780.5(1)	563.18(8)
Z		1	4	2
Density (X-ray) (g/cm^3)		7.83	7.41	7.36
Diffractometer			Stoe Stadi-P	
			MoK_α radiation, germanium monochromator	
θ range (°)			4–40	
No. of data points		1771	1744	1772
No. of reflections		48	574	414
Excluded regions (θ (°))			16.88–17.20	
			24.04–24.44	
			28.34–28.66	
Structure refinement			Gsas [27], Expgui [28]	
No. of structure parameters		3	11	9
No. of profile parameters			4	
No. of background parameters		18	25	28
R values	R_P	0.086	0.102	0.070
	R_{F^2}	0.044	0.075	0.068
Refinement plots			Fig. 1	

Table 3
Atomic coordinates and isotropic displacement parameters (pm^2) in (top down) $LaSn_3$ (Cu_3Au type), La_2Sn_5 (Ce_2Sn_5 type) and La_3Sn_7 (Gd_3Sn_7 type).

Atom	Wyckoff Position	*x*	*y*	*z*	$U_{iso.}$
$LaSn_3$:					
La(1)	1*a*	0	0	0	120(15)
Sn(1)	3*c*	0	1/2	1/2	120(15)
La_2Sn_5:					
La(1)	4*i*	0	0.2968(3)	0	85(11)
La(2)	4*i*	0	0.4324(4)	0	85(11)
Sn(1)	4*j*	0	0.2216(4)	1/2	217(7)
Sn(2)	4*i*	0	0.1382(3)	0	217(7)
Sn(3)	4*j*	0	0.3628(3)	1/2	217(7)
Sn(4)	4*j*	0	0.0719(4)	1/2	217(7)
Sn(5)	2*a*	0	0	0	217(7)
Sn(6)	2*c*	1/2	0	1/2	217(7)
La_3Sn_7:					
La(1)	4*i*	0	0.1871(3)	0	63(10)
La(2)	2*a*	0	0	0	63(10)
Sn(1)	4*j*	0	0.2882(4)	1/2	304(8)
Sn(2)	4*i*	0	0.4055(5)	0	304(8)
Sn(3)	4*j*	0	0.0946(5)	1/2	304(8)
Sn(4)	2*c*	1/2	0	1/2	304(8)

Wien2k [34]). The exchange-correlation contribution was described by the *generalized gradient approximation* (GGA) of *Perdew*, *Burke* and *Ernzerhof* [35]. Muffin-tin radii were chosen as 121.7 pm (2.3 a.u.) for all atoms. Cutoff energies used are $E_{max}^{pot} = 190$ eV (potential) and $E_{max}^{wf} = 170$ eV (interstitial PW). Electron densities and *Fermi* surfaces were calculated and visualized using the programs XCrysDen [36] and DrawXTL [37]. A *Bader* analysis of the electron density map was performed to evaluate both the charge distribution between the atoms and the bond critical points [38]. Further details and selected results of the calculations are summarized in Table 5. The total and selected partial Sn density of states are depicted in the Figs. 3 and 4. In Fig. 5, two selected cross sections of the valence electron density in La_2Sn_5 are shown.

4. Results and discussion

4.1. Compound formation and phase stabilities

While the congruently melting tristannide of lanthanum can be easily prepared from stoichiometric melts, the exact melting behavior of La_3Sn_7 and La_2Sn_5, which are not detected in any of the published phase diagrams [9–11], is a puzzling problem. The chemical compositions of the two stannides La_3Sn_7 and La_2Sn_5 (70 and 71.4% Sn content, respectively), are very closely related and furthermore coincide with the eutectic (70.5% Sn, T_e=1113 °C) between the congruently melting compounds La_3Sn_5 (T_M=1240 °C) and $LaSn_3$ (T_M=1155 °C). The respective cerium compounds Ce_2Sn_5 and Ce_3Sn_7 are assumed to decompose peritectically at temperatures close to the eutectic, but have been successfully prepared by annealing samples at 1090 (Ce_2Sn_5) and 1048 °C (Ce_3Sn_7) [26]. Our experimental data (s. Chapter 3.1) suggest, that the melting behavior of La_2Sn_5 and La_3Sn_7 is very similar. La_3Sn_7 (like Ce_3Sn_7) evidently shows a slightly lower peritectic temperature (*cf.* phase composition of sample 6a at a maximum temperature of 1050 °C) and can be thus best prepared by arc melting, quenching and subsequent annealing. The peritectic temperature of La_2Sn_5 is slightly increased and very close to the liquidus curve, the compound is thus also accessible from stoichiometric melts (*cf.* sample no. 3b). La_2Sn_5 has recently been confirmed in the course of a study of the ternary system La–Ag–Sn at only 400 °C [25]. The existence and melting behavior of the two phases La_2Sn_5 and La_3Sn_7 is evidently the reason for the unusual asymmetric form of the liquidus of $LaSn_3$ observed in [11].

4.2. Crystal structure description and comparison

The crystal structures in this series of tin-rich rare earth stannides ($LaSn_3$, La_3Sn_7 and La_2Sn_5) can be described as ordered variants of the cubic close sphere packing. Hence, all three compounds are crystallographic superstructures of the face-centered cubic lattice (f.c.c.). (Note, however, that La_3Sn_7 and La_2Sn_5 are not superstructures of $LaSn_3$). $LaSn_3$ with the Cu_3Au

structure type is related by the simple group-subgroup relation $Fm\bar{3}m \xrightarrow{k2} Pm\bar{3}m$ to the f.c.c. aristotype. For the orthorhombic structures of La_3Sn_7 ($oS20$) and La_2Sn_5 ($oS28$) a group-subgroup relation starting from the f.c.c. packing ($cF4$) is possible in two general steps: The first transformations are symmetry reductions of overall index 12 maintaining the unit cell: $Fm\bar{3}m \xrightarrow{t2} Fm\bar{3} \xrightarrow{t3} Fmmm \xrightarrow{k2} Cmmm$ [39,40]. In a second step, an enlargement of the unit cell in any of the former cubic axes by an index p, where p is an arbitrary prime number, is possible without a change in the space group (isomorphic symmetry reduction of index p: $Cmmm \xrightarrow{ip} Cmmm$ [39,41]). For the two structures of La_3Sn_7 and La_2Sn_5, this enlargement occurs in the b direction with p indices 5 and 7, respectively. Because of the significant distortion of the observed structures (see below) the b/a and b/c axis ratios exceed these ideal factors p by 0.6–0.75 (La_3Sn_7: 5.74/5.61; La_2Sn_5 7.72/7.52). As detailed below, these crystallographic symmetry relations alone are interesting in their own right but not sufficient for the understanding of the chemical bonding in these compounds.

The tristannide $LaSn_3$ (Cu_3Au structure type) is isotypic to $CaSn_3$ and the rare earth tristannides from lanthanum up to erbium; from Gd to Tm the Gd_4Sn_{11} structure exists in addition. Due to the electronic structure and bonding situation (*cf.* Chapter 4.3) the structure of $LaSn_3$ can be alternatively described as a network of [Sn_6] octahedra (*closo* clusters) connected via common vertices (Fig. 2a). The Sn–Sn bond length **e** is 338 pm (*cf.*335.2 pm for $CaSn_3$), both atom types show a cuboctahedral coordination (Table 4).

Fig. 2b demonstrates the common structural principle for the family of compounds with the general formula $La_{n+1}Sn_{3n-2}$ or $La_{m+1}Sn_{3m+1}$. Here, the octahedra network of $LaSn_3$ is sliced every m layers perpendicular to the b direction and the resulting blocks are sheared along a vector $\frac{1}{2}y,0$, preserving the orthorhombic symmetry only. As a consequence of the $x=\frac{1}{2}$ shift, identity along the stacking direction is reached after two blocks, C centering and the *mmm* crystal class are preserved. In between any two blocks, one formula unit of LaSn (gray box in Fig. 2b; CrB structure type, space group *Cmcm*, $a=478.2$, $b=1194$, $c=442.2$ pm [9]) is interspersed. This is possible, because both the unit cell dimension a (478.2 pm), *i.e.* the distance between the planar zigzag chains, and the translation period along the chains ($c=442.2$ pm) are compatible with the lattice parameter of $LaSn_3$ ($a=477.77(1)$ pm). While the coordinates of the 'cut' La atoms (La(1)) of the $LaSn_3$ blocks fit both the $LaSn_3$ and the CrB structure, the 'cut' tin tips (Sn(1)) of the octahedra are shifted by approximately 40 pm into the interior of the CrB layers (small arrows in Fig. 2b). As a first consequence, these Sn(1) atoms exhibit short Sn–Sn distances among each other ($d_{Sn(1)-Sn(1)} = 305-308$ pm, bond length **a**, Table 4) and, like in LaSn, they are coordinated by six lanthanum atoms in a trigonal prismatic arrangement. As a second consequence, no bonding interaction of Sn(1) with 'its' octahedron is left ($d_{Sn(1)-Sn(2,3)} = 380$ pm) and the polyhedra terminating the $LaSn_3$ blocks are reduced to square pyramids (Figs. 2c and d). Cutting every third octahedra layer ($m=3$) results in $3 \times LaSn_3 + LaSn = La_4Sn_{10} = 2 \times La_2Sn_5$ (Fig. 2c), cutting every second layer ($m=2$) in $2 \times LaSn_3 + LaSn = La_3Sn_7$ (Fig. 2d) and the whole structure series may be best addressed as $m \times LaSn_3 + LaSn = La_{m+1}Sn_{3m+1}$. A comparable structural principle is found in the perovskite-like crystals of the Ruddlesden–Popper series $(ABX_3)_n(AX)_m$ with the insertion of half a NaCl unit cell (AX) in between the perovskite blocks ABX_3, shifted by $\frac{1}{2}$, $\frac{1}{2}$, z, in this case maintaining the tetragonal body centered symmetry. The related alternative description of the structure series of the tin-rich stannides as an intergrowth of

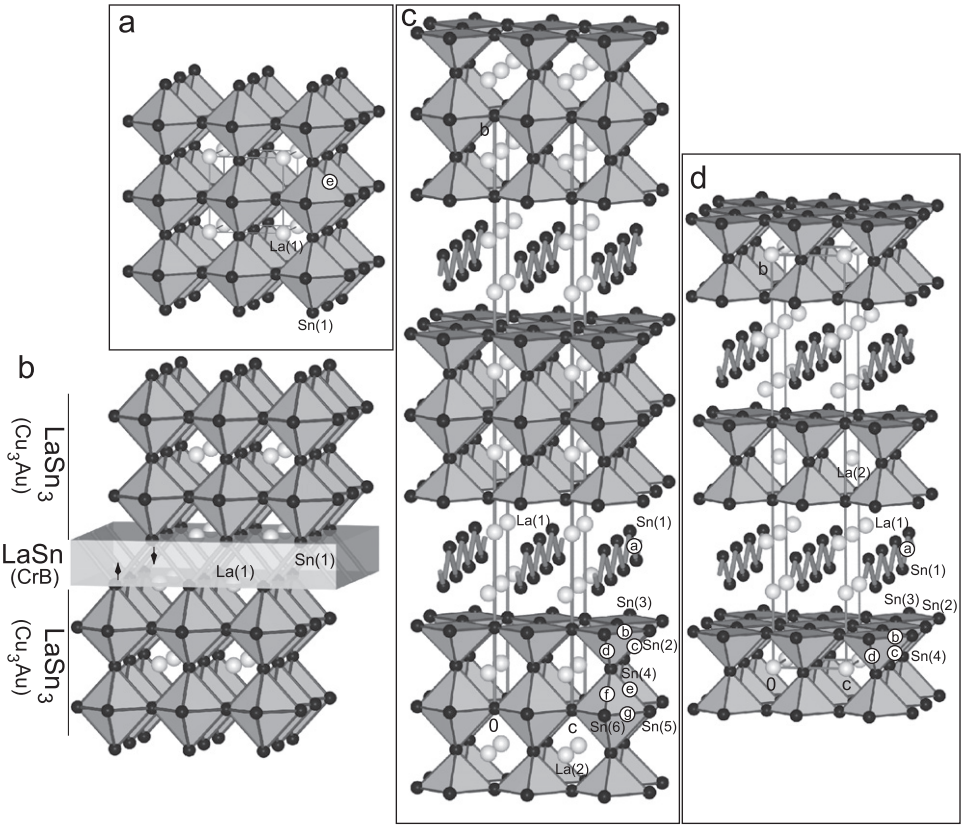

Fig. 2. Polyhedra representations of the crystal structures of $LaSn_3$ (Cu_{3Au} structure type, (a), La_2Sn_5 (Ce_2Sn_5 type, c) and La_3Sn_7 (Gd_3Sn_7 type d) together with (b) the principle of cutting and shearing $LaSn_3$ and intercalating LaSn (CrB) (Large light gray spheres: La; small dark spheres Sn; polyhedra: *closo*-[Sn_6] octahedra and *nido*-[Sn_5] square pyramids [37]. s. Table 4 for the marked Sn–Sn distances).

Table 4
Selected interatomic distances (pm) in $LaSn_3$ (above), La_2Sn_5 (middle) and La_3Sn_7 (below).

Atoms		Distance	No.	Mult.	CN	Atoms		Distance	No.	Mult.	CN
$LaSn_3$:											
La	−Sn	337.8(1)	*e*	12 ×	12	Sn	- Sn	337.8(1)	*e*	8 ×	
							−La	337.8(1)		4 ×	8+4
La_2Sn_5:											
La(1)	−Sn(2)	329(1)		2 ×		La(2)	−Sn(4)	330.5(1)		4 ×	
	−Sn(3)	333(1)		2 ×			−Sn(5)	335(1)		2 ×	
	−Sn(1)	336.7(3)		4 ×			−Sn(6)	337.4(9)		2 ×	
	−Sn(1)	357.4(5)		2 ×			−Sn(3)	343(1)		2 ×	
	−La(1)	408(2)		2 ×	10+2		−Sn(2)	343(1)		2 ×	12
Sn(1)	−Sn(1)	308(2)	*a*	2 ×		Sn(2)	−Sn(3)	330.1(3)	*b*	4 ×	
	−La(1)	336.7(3)		4 ×			−Sn(4)	334(1)	*c*	2 ×	
	−La(1)	357.4(5)		2 ×	2+6		−La(1)	329(1)		2 ×	
							−La(2)	343(1)		2 ×	6+4
Sn(3)	−Sn(4)	329(1)	*d*	2 ×		Sn(4)	−Sn(3)	329(1)	*d*	2 ×	
	−Sn(2)	330.1(1)	*b*	4 ×			−Sn(2)	334(1)	*c*	2 ×	
	−La(1)	333(1)		2 ×			−Sn(5)	349(1)	*e*	2 ×	
	−La(2)	343(1)		2 ×	6+4		−Sn(6)	347(1)	*f*	2 ×	
							−La(2)	330.5(1)		4 ×	8+4
Sn(5)	−Sn(6)	330.1(3)	*g*	4 ×		Sn(6)	−Sn(5)	330.1(1)	*g*	4 ×	
	−Sn(4)	349(1)	*e*	4 ×			−Sn(4)	347(1)	*f*	4 ×	
	−La(2)	335(1)		4 ×	8+4		−La(2)	337.4(9)		4 ×	8+4
La_3Sn_7:											
La(1)	−Sn(1)	333.8(3)		4 ×		La(2)	−Sn(4)	327.3(1)		4 ×	
	−Sn(2)	334(1)		2 ×			−Sn(2)	338(1)		4 ×	
	−Sn(3)	337(1)		2 ×			−Sn(3)	341.4(9)		4 ×	12
	−Sn(1)	354(1)		2 ×							
	−La(1)	403(1)		2 ×	10+2						
Sn(1)	−Sn(1)	305(2)	*a*	2 ×		Sn(2)	– Sn(3)	327.3(1)	*b*	4 ×	
	−La(1)	333.8(3)		4 ×			−Sn(4)	341(1)	*c*	2 ×	
	−La(1)	354(1)		2 ×	2+6		−La(1)	334(1)		2 ×	
							−La(2)	338(1)		2 ×	6+4
Sn(3)	−Sn(2)	327.3(1)	*b*	4 ×		Sn(4)	−Sn(2)	341(1)	*c*	4 ×	
	−Sn(4)	338.9(9)	*d*	2 ×			−Sn(3)	337.9(9)	*d*	4 ×	
	−La(1)	337(1)		2 ×			−La(2)	327.3(1)		4 ×	8+4
	−La(2)	341.4(9)		2 ×	6+4						

fragments of Cu_3Au, CaF_2 and AlB_2 [42,43] neglects some of the features of the chemical bonding in the Sn polyanion (s. Chapter 4.3).

In La_2Sn_5 (Fig. 2c, Ce_2Sn_5 structure type [26]) one layer of *closo* octahedra, formed by Sn(4) to Sn(6), is preserved. The Sn–Sn distances in this region of the structure (bonds **e**, **f** and **g**, $d_{Sn-Sn} = 330-348$ pm, Table 4) are similar to the value of **e** in the basic structure of $LaSn_3$ (338 pm). As in $LaSn_3$, the atoms La(2) and Sn(4) to Sn(6) situated in this part of the structure are cuboctahedrally coordinated by 12 Sn and 8 Sn+4 La atoms. The Sn–Sn distances in the square pyramids (*nido* clusters, 'cut' octahedra), *i.e.* bonds **b**, **c** and **d** (329–334 pm) are slightly decreased when compared to $LaSn_3$. In the structure of the binary stannide La_3Sn_5 with the nearly isolated Sn_5 *nido* clusters the Sn–Sn bond lengths are further decreased (303–323 pm, [15]). The coordination sphere of Sn(2) and Sn(3) forming the terminating square net is reduced to 6+4 for Sn+La. The Sn(1)–Sn(1) distance in the zigzag chains of the CrB (LaSn) section of the La_2Sn_5 structure are the strongest Sn–Sn bonds in the structure, exhibiting a value of 308 pm. The Sn–Sn–Sn bond angle in the chain is 97.6°. For the reference compound LaSn only the lattice parameters are known from powder data. Using the atomic parameters of CaSn [44], the Sn–Sn distance calculates to 298 pm and the intra-chain angle to 95.6°. The further coordination of Sn(1) is also comparable with LaSn: six La atoms at distances between 330 and 357 pm form stretched trigonal prisms, as observed for all electron rich members of the CrB series.

In the structure of La_3Sn_7 (Fig. 2d) no complete octahedra layer of $LaSn_3$ is retained, leaving only two layers of square pyramids. In between these double layers the Sn zigzag chains are located. As a consequence, only La(2) and Sn(4) show the full cuboctahedral coordination. Like in La_2Sn_5, Sn(2) and Sn(3) exhibit a 6+4 coordination. The Sn–Sn distances in the square pyramids are likewise in the range 327–341 pm. The Sn(1)–Sn(1) intra-chain bond length (305 pm) and the coordination of Sn(1) (details s. Table 4 bottom) are also identical. According to the above description of the structure series, La_2Sn_5 can reversely be described as La_3Sn_7 with an extra $LaSn_3$ layer of complete Sn_6 octahedra inserted.

$LaSn_2$ ($ZrGa_2$ type [12]) is the last link of the structural series $La_{m+1}Sn_{3m+1}$ with $m=1$. The reported lattice parameters of $LaSn_2$ based on powder data of an annealed sample ($a=442.7(1)$, $b=1585.5(4)$, $c=451.4(1)$ pm) and the volume of 316.8×10^{-6} pm^3 perfectly fit the 1:2 La stannide of this series, where only square planar nets are left in between the Sn zigzag chains (in [12] the Nd and the Sn(1) position of $NdSn_2$ are accidentally interchanged). As the formation of this compound was never observed in this work and in several other systematic studies of the La–Sn system [9–11], no further discussion on this phase is possible at present.

The structure type of La_2Sn_5 is observed not only for the cerium and lanthanum stannide but is assigned to powder patterns of the other early rare earth stannides up to samarium too. In contrast, the late lanthanoid stannides of Ho to Lu of same stoichiometry form the Er_2Ge_5 structure type. The structure type

Table 5
Details of the calculation of the electronic structures of $CaSn_3$, $LaSn_3$, La_2Sn_5 and La_3Sn_7.

			$CaSn_3$	$LaSn_3$	La_2Sn_5	La_3Sn_7
Structure type			Cu_3Au		Ce_2Sn_5	Gd_3Sn_7
Crystal data			[33]		Tables 2 and 3	
R_{mt} (all atoms)			121.7 pm (2.3 a.u.)			
$R_{mt} \cdot K_{max}$			8.0			
k-points/BZ			1000		900	
k-points/IBZ			35		150	
Monkhorst-Pack-Grid			$10 \times 10 \times 10$		$10 \times 10 \times 9$	
DOS plot			Fig. 3		Fig. 4	
Bader charge		Ca/La(1)	+1.251	+1.212	+1.202	+1.216
		La(2)	–	–	+1.211	+1.189
		Sn(1)	−0.417	−0.404	−0.756	−0.764
		Sn(2)	–	–	−0.415	−0.439
		Sn(3)	–	–	−0.425	−0.419
		Sn(4)	–	–	−0.396	−0.378
		Sn(5)	–	–	−0.430	–
		Sn(6)	–	–	−0.416	–
		Bond No.				
ρ_{BCP}	Sn–Sn	**a**	–	–	0.224 (308.3)	0.237 (304.6)
		b	–	–	0.171 (330.1)	0.177 (327.3)
		c	–	–	0.164 (334.0)	0.152 (341.3)
		d	–	–	0.173 (329.3)	0.156 (337.9)
		e	0.156 (335.2)	0.156 (337.8)	0.139 (348.5)	–
		f	–	–	0.141 (346.5)	–
		g	–	–	0.172 (330.1)	–
	Sn–La/Ca	max.	0.094 (335.2)	0.144 (337.8)	0.170 (329)	0.165 (327)
					La(1)–Sn(2)	La(2)–Sn(4)

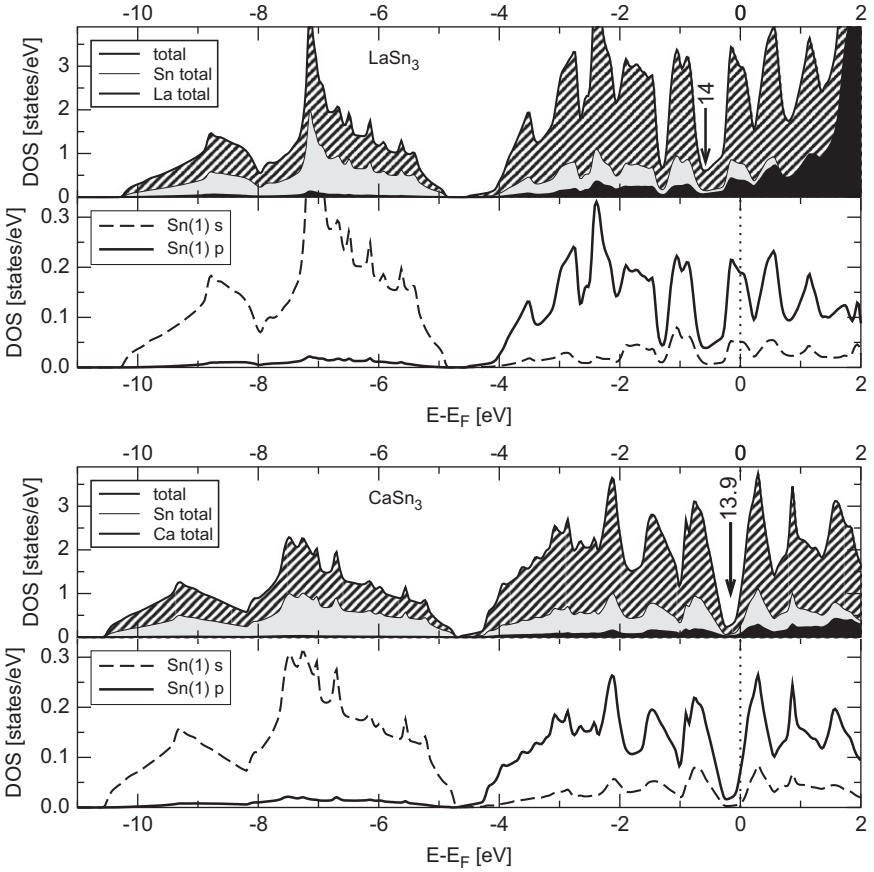

Fig. 3. Calculated total (top) and partial (bottom) density of states in $LaSn_3$ and $CaSn_3$ (black: La/Ca pDOS; gray: Sn pDOS). Arrows indicate selected minima of the tDOS in v.e./f.u.

of La_3Sn_7, which is denoted in the literature as Gd_3Sn_7 [30] or Ce_3Sn_7 [26] type is observed for the rare earth elements La to Tb [42] and also for the high pressure forms of the respective Ho and Er stannides [43]. The $ZrGa_2$ type structure of $LaSn_2$ is also assigned to the early lanthanum distannides $PrSn_2$, $NdSn_2$ [45] and $SmSn_2$ [12], whereas the late rare earth elements form the $ZrSi_2$ structure type instead.

4.3. Chemical bonding and electronic structure

Because of its superconducting properties, the chemical bonding and electronic structure of $LaSn_3$ have been a subject of research since the early seventies. As early as 1972, theoretical band structure calculations using the MOPW (modified orthogonalized-plane-wave) method have been performed [21,22]. In 1982, the LMTO method has been applied to the problem and the Fermi surface was further investigated by De-Haas-van Alphen effect measurements [20,21]. This calculation showed, that the La-4*f* states are situated fully above the Fermi level. In contrast, 5*d* states play a significant role in the chemical bonding, contributing 26% of the total density of states (tDOS) at E_F (52% Sn-*p* proportion). In the present work, the electronic structures of the three tin-rich lanthanum stannides were studied in the framework of the FP-LAPW method (*cf.* Chapter 3.4 and Table 5). The calculated total and partial La and Sn density of states (tDOS/pDOS) of $CaSn_3$ and the lanthanum stannides are depicted in the Figs. 3 and 4.

Fig. 3 compares the tDOS and pDOS of the calcium tristannide and the isotypic lanthanum compound, the latter being in good accordance with the results of the LMTO calculation by Boulet, Jan and Skriver [20]. Most of the features of the tDOS and also the band structure itself are very similar between both compounds. Due to the difference in the valence electron numbers, the pronounced minimum in the tDOS of $CaSn_3$ coincides with the

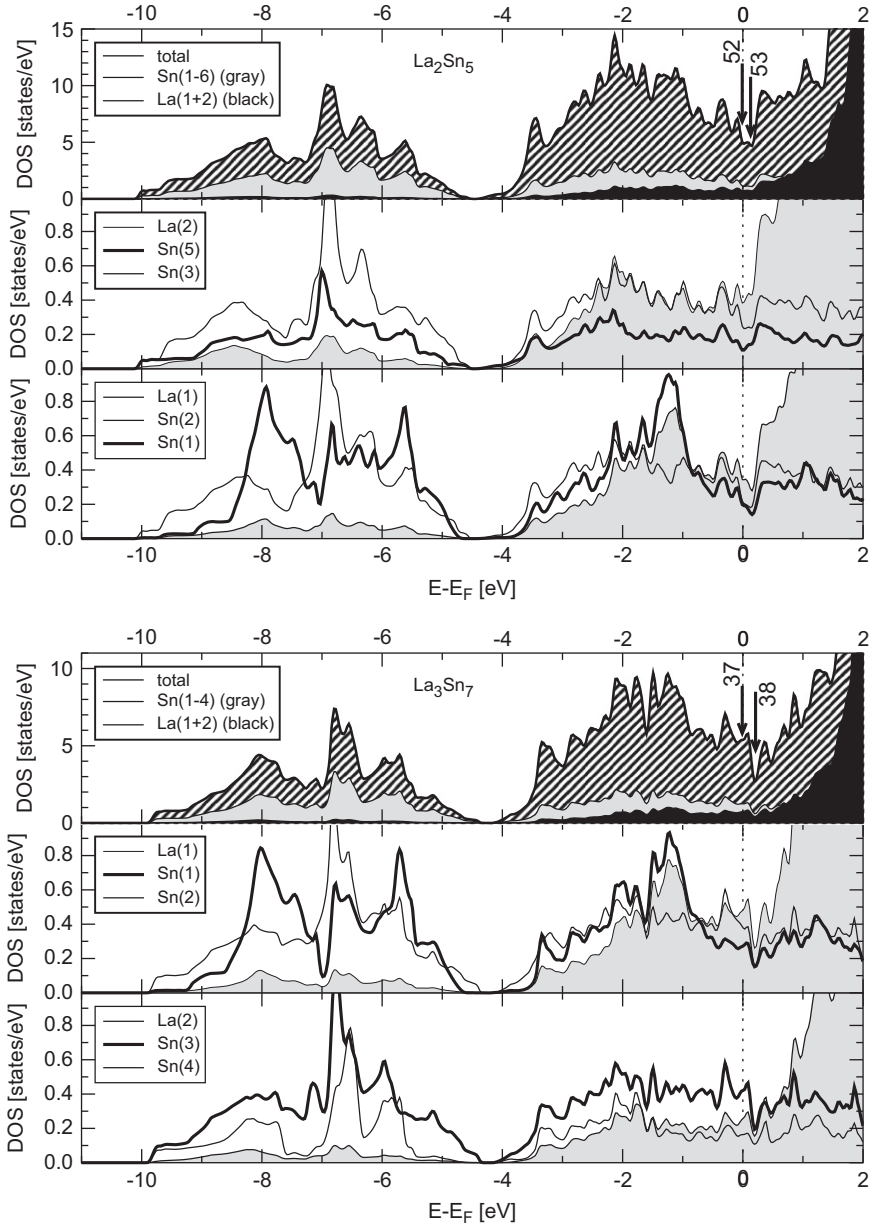

Fig. 4. Calculated total (top; black: La pDOS) and partial La/Sn (bottom; gray: La) density of states in La_2Sn_5 and La_3Sn_7. Arrows indicate selected minima of the tDOS in v.e./f.u.

Fermi level (E_F), whereas it is located slightly below E_F in the case of $LaSn_3$. By substituting tin against indium, the Fermi level can be moved back into the *pseudo* band gap and the expected dramatic changes of several physical properties (superconducting critical temperature, specific heat, susceptibility) and NMR parameters have already been analyzed [23]. The second difference between $CaSn_3$ and $LaSn_3$ is the amount of electron transfer from the electropositive metal towards tin (black filled curves in the upper parts of Fig. 3). As already mentioned above in context of the prior LMTO calculation, it is mainly the *d* electrons of lanthanum that are not fully transferred to the stannide polyanion. This also comes apparent from the Bader charge, which – despite the difference in v.e. numbers – is very similar in both compounds (Ca: +1.251; La: +1.212, Table 5). This in reverse means, that La-*d* states are strongly involved in the bonding and the bond critical points observed between La and Sn are nearly of equal heights when compared to the values of the Sn–Sn contacts, whereas they are much smaller in the case of the alkaline earth compounds (Table 5). The same difference between isotypic compounds of the alkaline earth elements and lanthanum has been observed for the cluster compounds forming the Pu_3Pd_5 structure type [15,46,47].

The pronounced *pseudo* band gaps in the electronic structures of simple alkaline earth tritetrelides like $CaSn_3$ and $CaPb_3$ (14 v.e./f.u.) crystallizing with the Cu_3Au type can be used as the starting point for the delineation of stannides [6,7] and plumbides [48] using the electron counting rules of Zintl and Wade/Jemmis. In $CaSn_3$ the charge transfer Ca → Sn is next to complete and also comparable to that in electron precise classical Zintl phases [49]. When taking the Sn–Sn contacts in the region 330–340 pm into account, the structure of $CaSn_3$ can be described as above, *i.e.* consisting of *closo* clusters $[Sn_6]^{4-}$, which are connected in such a way, that each tin atom participates in two vertex-sharing octahedra. The $4\frac{2}{3}$ v.e./Sn (14 v.e./f.u.) are thus distributed among two *closo* clusters, so that – just like in the electron precise borides with *closo* clusters like CaB_6 – each cluster atom contributes $2\frac{1}{3}$ v.e. to each *closo* cluster. Irrespective of this interpretation as covalent polyanionic network, $CaSn_3$ is of course a metal and the band structure exhibits features (*e.g.* bands of high dispersion crossing E_F) that are characteristic for metallic bonding (*cf.* discussion in [6]).

In $LaSn_3$, the tDOS minimum is also found at about 14 v.e. A simple analysis of the Sn-*p* bonding is thus sufficient to explain the main features of the tDOS. However, the difference between $CaSn_3$ and $LaSn_3$ is not only the shift of the Fermi level from the *pseudo* band gap towards a higher tDOS, but also the significantly larger contribution of La states to the tDOS, in fact already below the limit of 14 v.e. (black regions in Fig. 3). Clearly the lanthanum species cannot be simply La^{2+}, like Ca^{2+} in the calcium compound, but the remaining La electrons provoke strong La–Sn bonding contributions. This comes apparent from the significantly increased bond critical points (BCPs) between La and Sn (0.144 e^-10^{-6} pm^{-3} compared to 0.094 e^-10^{-6} pm^{-3} in $CaSn_3$), whereas the values at the Sn–Sn bonds are identical in the two tristannides ($\rho_{BCP} = 0.156$ e^-10^{-6} pm^{-3}).

The tDOS of the two other stannides, La_2Sn_5 and La_3Sn_7, (Fig. 4) also exhibit pronounced minima, which in these cases are situated slightly above the Fermi level (38 v.e./f.u. compared to 37 v.e. present in La_3Sn_7 and 52–53 v.e./f.u. compared to 52 v.e. in La_2Sn_5). In LMTO-ASA calculations of the isotypic compounds Ce_3Sn_7 [50] and Er_3Sn_7 [43] a similar minimum is discernible, although it is somewhat hidden by the large DOS of the Ce/Er *f* states at E_F. As for $LaSn_3$, a similar simple electron count according to the Zintl concept and Wade's rules, based on the observed anionic partial structure, is able to explain these pronounced minima. According to the increased v.e. number per tin, the condensed *closo* clusters of $LaSn_3$ ($\frac{14}{3} = 4.67$ v.e./Sn) are disintegrated into more electron demanding *nido* clusters and even two-bonded Sn^{2-} (like in CaSn) with 6 v.e./Sn. These Sn(1) atoms of the zigzag chains have to be counted with an electron demand of 6 v.e., because they are two-bonded according to the 8-*N* rule. Tin atoms participating in two octahedra are counted like those in the tristannides, *i.e.* $2(1/3) = 7/3$ v.e. per cluster. Due to the fact that the *nido* clusters (square pyramids Sn_5) require 14 v.e. ($N+2$ v.e. pairs) according to Wade's rule, each vertex can be assigned a demand of $\frac{14}{5}$ v.e. per cluster. For La_2Sn_5 the overall v.e.

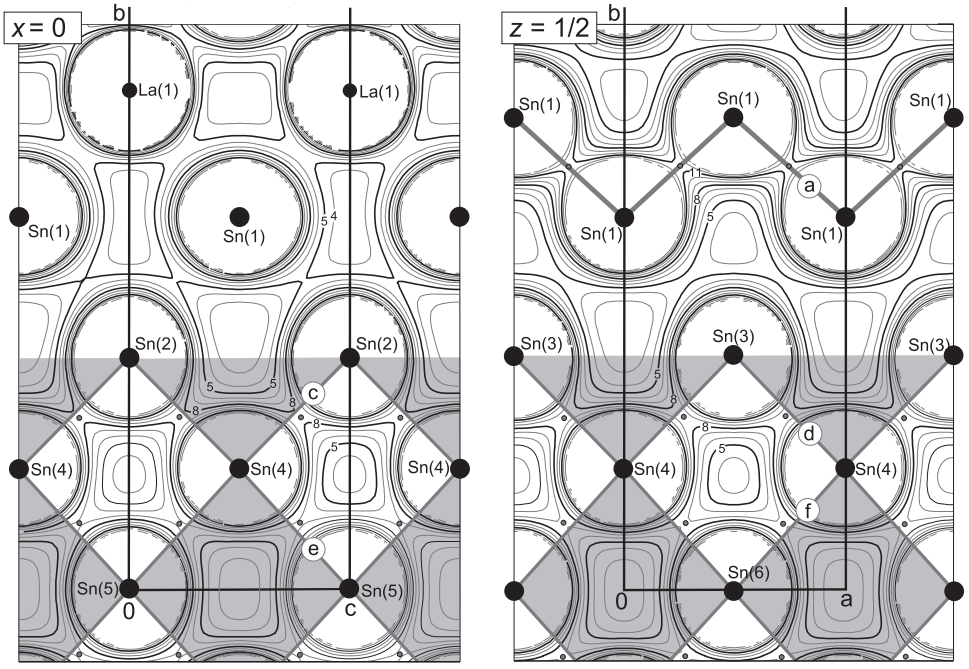

Fig. 5. Cross-section of the valence electron density of La_2Sn_5. (Values between 0.0 and 0.3 e^-10^{-6} pm^{-3} with iso-lines drawn in steps of n with $n \times 0.02$ e^-10^{-6} pm^{-3}).

requirement thus sums up to

$$\underbrace{2\times 6}_{\mathrm{Sn(1)}}+\underbrace{\frac{8}{2}\times\left(\frac{14}{5}+\frac{14}{5}\right)}_{\mathrm{Sn(2,3)}}+\underbrace{2\times\left(\frac{7}{3}+\frac{14}{5}\right)}_{\mathrm{Sn(4)}}+\underbrace{\frac{4}{2}\times\left(\frac{7}{3}+\frac{7}{3}\right)}_{\mathrm{Sn(5/6)}}=54.$$

The analogous calculation for the second compound, La_3Sn_7, is

$$\underbrace{2\times 6}_{\mathrm{Sn(1)}}+\underbrace{\frac{8}{2}\times\left(\frac{14}{5}+\frac{14}{5}\right)}_{\mathrm{Sn(2,3)}}+\underbrace{1\times\left(\frac{14}{5}+\frac{14}{5}\right)}_{\mathrm{Sn(4)}}=40.$$

Both calculated values are very close to the observed *pseudo* band gaps at 52–53 and 38 v.e./f.u., which are themselves identical to or only slightly higher than the observed number of valence electrons (52 and 37 v.e./f.u.). The small deviations to higher v.e. numbers are easily explained by the fact, that the tetrelides of the CrB type are known to exhibit considerable phase widths and are stable also with up to 0.5 v.e./f.u. less. As for $LaSn_3$, the simple consideration of exclusively Sn-*p* bonding is thus able to explain the minima of the tDOS close to E_F. Again, this simplified scheme neglects the large Sn–La bonding contributions (and thus the amount of electron transfer from La to Sn). Even more pronounced than in $LaSn_3$, the 2:5 and 3:7 stannides exhibit high electron densities and distinct bond critical points between La and Sn, which now equal the values of the Sn–Sn contacts in the $LaSn_3$-analogous parts of their structures.

The Bader charges of the tin atoms are in general accordance with the interpretation after Zintl/Wade showing the same tendencies as the above calculated formal charges: The most negative charge of −0.76 is observed for the Sn(1) atoms of the zigzag chains. The Sn atoms of the square pyramids terminating the $LaSn_3$ blocks bear an intermediate negative charge (Sn(2/3): −0.41 to −0.44) and the charge of the atoms in the $LaSn_3$ blocks is further increased and fits the values of $LaSn_3$ itself (−0.38 to −0.43). The details of the valence electron distribution (see cross sections for La_2Sn_5 in Fig. 5) as well as the ELI (electron localizability indicator) analysis of an LTMO-ASA calculation of Er_3Sn_7 [43] are also consistent with this interpretation: All Sn–Sn edges of the tin polyhedra show distinct bond critical points of about 0.14 to 0.18 e^-10^{-6} pm^{-3}, with the individual values correlating with the Sn–Sn bond lengths (Table 5). The ELI distribution of Er_3Sn_7 exhibits a 5*c* Sn_5 attractor inside the *nido* cluster. The shortest and strongest Sn–Sn bonds in the structures are the bonds **a**, which also carry the highest bond critical points ($\rho_{BCP}=0.22-0.24$ e^-10^{-6} pm^{-3}). No BCSs (and also no ELI attractors in Er_3Sn_7) are found between the Sn(1) atoms of the chain and the *nido* clusters (Sn(2,3)). The explicit BCPs between La and Sn, especially in the CrB regions of the structure, correspond to ELI attractors like Sn(1)Er_3 and account for the significant participation of La *d* states in the overall chemical bonding in these types of polar intermetallic compounds.

4.4. Summary and conclusion

The stannides La_2Sn_5 and La_3Sn_7 are interesting members of the series of compounds $La_{m+1}Sn_{3m+1}$, not only because of their puzzling melting behavior, but also due to their interesting chemical bonding. Aspects of metallic (the structures are superstructures of a f.c.c. packing) and covalent bonding contributions are equally crucial. The revised crystal structure description highlights the Sn–Sn bonding, *i.e.* the polyanionic character of the compounds, by taking Sn–Sn bonds up to 350 pm into account, which all carry bond critical points in the calculated valence electron densities. For the resulting building blocks (*closo*/*nido* clusters and zigzag chains), the v.e. count after Zintl and Wade fits the observed v.e. numbers almost exactly and thus also coincides with the minima of the tDOS at or near the Fermi level. Compared to the calcium and strontium stannides, *d* states of the cations are strongly involved in the chemical bonding. This may be seen as a reason for the singular structural chemistry of the rare earth stannides for which there is no equivalent among the respective alkaline earth compounds.

Acknowledgments

We would like to thank the *Deutsche Forschungsgemeinschaft* and the *Adolf-Messer-Stiftung* for financial support.

Appendix A. Supplementary data

Supplementary data associated with this article can be found in the online version at doi:10.1016/j.jssc.2011.06.035.

References

[1] H. Schäfer, B. Eisenmann, W. Müller, Angew. Chem. 85 (1973) 742.
[2] J.D. Corbett, Chem. Rev. 85 (1985) 383.
[3] S.M. Kauzlarich (Ed.) Chemistry, Structure, and Bonding of Zintl Phases and Ions, VCH Verlagsgesellschaft mbH, Weinheim, 1996.
[4] K. Wade, Adv. Inorg. Chem. Radiochem. 18 (1976) 1.
[5] E.D. Jemmis, M.M. Balakrishnarajan, P.D. Pancharatna, Chem. Rev. 102 (2002) 93.
[6] M. Wendorff, C. Röhr, Z. Anorg, Allg. Chem. 637 (2011) 1013.
[7] M. Wendorff, C. Röhr, Z. Naturforsch. 66b (2011) 245.
[8] R.D. Shannon, Acta Crystallogr. A 32 (1976) 751.
[9] V.N. Eremenko, M.V. Bulanova, P.S. Matsenyuk, V.E. Listovnichy, Dopov. Akad. Nauk Ukr. RSR, Geol., Khim., Biol. B 9 (1988) 35.
[10] A. Palenzona, S. Cirafici, J. Phase Equilibria 13 (1992) 42.
[11] M. Huang, X. Su, F. Yin, P. Zhang, Z. Li, C. Chen, J. Alloys Compd. 309 (2000) 147.
[12] F. Weitzer, K. Hiebl, P. Rogl, J. Solid State Chem. 98 (1992) 291.
[13] G. Borzone, A. Borsese, R. Ferro, Z. Anorg. Allg. Chem. 501 (1983) 199.
[14] M. Bonnet, J.X. Boucherle, F. Givord, F. Lapierre, P. Lejay, J. Odin, A.P. Murani, J. Schweizer, A. Stunault, J. Magn. Magn. Mater. 132 (1994) 289.
[15] M.T. Klem, J.T. Vaughey, J.G. Harp, J.D. Corbett, Inorg. Chem. 40 (2001) 7020.
[16] M.L. Fornasini, P. Manfrinetti, A. Palenzona, S.K. Dhar, Z. Naturforsch. 58b (2003) 521.
[17] J.D. Corbett, E. Garcia, A.M. Guloy, W.-M. Hurng, Y.-U. Kwon E.A. Leon-Escamilla, Chem. Mater. 10 (1998) 2824.
[18] Y.-U. Kwon, M.A. Rzeznik, A. Guloy, J.D. Corbett, Chem. Mater. 2 (1990) 546.
[19] I. Dürr, C. Röhr, in preparation.
[20] R.M. Boulet, J.-P. Jan, H.L. Skriver, J. Phys. F: Met. Phys. 12 (1982) 293.
[21] D.M. Gray, L.V. Meisel, Phys. Rev. B 5 (1971) 1308.
[22] D.M. Gray, L.V. Meisel, Phys. Rev. B 5 (1971) 1299.
[23] A.M. Toxen, R.J. Bamgino, L.B. Welsh, Phys. Rev. B 8 (1973) 90.
[24] B. Stalinski, Z. Kletowski, Z. Henkie, Phys. Stat. Sol. a 19 (1973) K165.
[25] J. Liang, C. Liao, Y. Du, Y. Tang, Y. Han, Y. He, S. Liu, J. Alloys Compd. 493 (2010) 122.
[26] J.X. Boucherle, F. Givord, P. Lejay, J. Schweizer, A. Stunault, Acta Crystallogr. B 44 (1988) 377.
[27] A.C. Larson, R.B.V. Dreele, General Structure Analysis System (GSAS), Los Alamos National Laboratory Report LAUR 86-748, 2000.
[28] B.H. Toby, J. Appl. Crystallogr. 34 (2001) 210.
[29] I.R. Harris, G.V. Raynor, J. Less-Common Met. 9 (1965) 7.
[30] R.V. Skolozdra, L.G. Akzelrud, V.K. Pecharsky, O.E. Koretskaya, Dopov. Akad. Nauk. Zkr. RSR, Geol., Khim., Biol. B 12 (1986) 48.
[31] G.M. Sheldrick, Shelxl-97—Program for the Refinement of Crystal Structures, University of Göttingen, Germany, 1997.
[32] G.M. Sheldrick, Acta Crystallogr. A 64 (2008) 112.
[33] A. Palenzona, P. Manfrinetti, M.L. Fornasini, J. Alloys Compd. 312 (2000) 165.
[34] P. Blaha, K. Schwarz, G.K.H. Madsen, D. Kvasnicka, J. Luitz, Wien2k—An Augmented Plane Wave and Local Orbital Program for Calculating Crystal Properties TU Wien, ISBN3-9501031-1-2, 2006.
[35] J.P. Perdew, S. Burke, M. Ernzerhof, Phys. Rev. Lett. 77 (1996) 3865.
[36] A. Kokalj, J. Mol. Graphics Modelling 17 (1999) 176.
[37] L.W. Finger, M. Kroeker, B.H. Toby, J. Appl. Crystallogr. 40 (2007) 188.
[38] R.W.F. Bader, Atoms in Molecules. A Quantum Theory, International Series of Monographs on Chemistry Clarendon Press, Oxford, 1994.
[39] E. Kroumova, J.M. Perez-Mato, M.I. Aroyo, S. Ivantchev, G. Madariaga, H. Wondratschek, The Bilbao Crystallographic Server: a web site with crystallographic tools using the International Tables for Crystallography in 18th European Crystallographic Meeting, 1998.
[40] T. Hahn (Ed.) International Tables for Crystallography. Vol A: Space-Group Symmetry International Union of Crystallography, 1985.

[41] H. Wondratschek, U. Müller (Ed.) International Tables for Crystallography. Volume A1, 2nd Edition, Symmetry Relations Between Space Groups, Wiley, 2010.
[42] A. Palenzona, P. Manfrinetti, J. Alloys Compd. 201 (1993) 43.
[43] K. Meier, L. Vasylechko, R. Cardoso-Gil, U. Burkhardt, W. Schnelle, M. Schmidt, Y. Grin, U. Schwarz, Z. Anorg. Allg. Chem. 636 (2010) 1695.
[44] W. Rieger, E. Parthé, Acta Crystallogr. 22 (1967) 919.
[45] A. Saccone, D. Maccio, R. Ferro, J. Alloys Compd. 201 (1993) L9.
[46] I. Dürr, M. Schwarz, M. Wendorff, C. Röhr, J. Alloys Compd. 494 (2010) 62.
[47] I. Dürr, C. Röhr, Z. Anorg. Allg. Chem. 636 (2010) 368.
[48] M. Wendorff, C. Röhr, Z. Naturforsch. 63b (2008) 1383.
[49] W. Harms, M. Wendorff, C. Röhr, J. Alloys Compd. 469 (2009) 89.
[50] J. Goraus, A. Slebarski, M. Neumann, J. Alloys Compd. 401 (2005) 189.